ACS OMEGA

Open Access

This article is licensed under CC-BY-NC-ND 4.0

http://pubs.acs.org/journal/acsodf

Article

Split-crRNA Transcription Based Dual-Recognition Cascade Amplification Assay for Sensitive and Accurate Postoperative Delirium Related MicroRNA Analysis

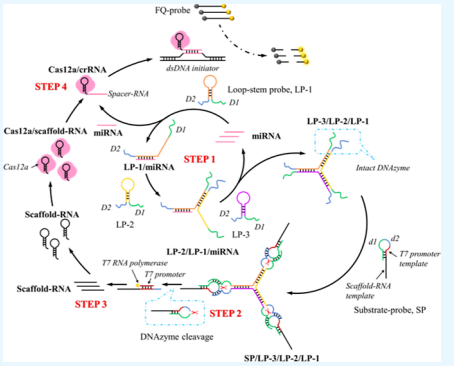
Lihua Wang, Huihui Li, Kai Wang, Jinge Ma, Guosheng Liu, Ning Li, and Baojun Zhang*

Cite This: *ACS Omega* 2026, 11, 24705−24713

Read Online

ACCESS | Metrics & More | Article Recommendations | Supporting Information

ABSTRACT: Postoperative delirium (POD) represents a serious neuropsychiatric complication, underscoring the urgent need for sensitive and specific detection of circulating microRNAs (miRNAs) as potential biomarkers. Conventional isothermal amplification methods, however, often face a trade-off between sensitivity and specificity. Herein, we report a cascade amplification strategy that integrates catalytic hairpin assembly (CHA), split DNAzyme cleavage, T7 RNA polymerase-mediated transcription, and CRISPR-Cas12a *trans*-cleavage to achieve ultrasensitive and accurate miRNA detection. The design is centered on a dual-recognition mechanism: the same target miRNA molecule first initiates the CHA cascade to reassemble an active split DNAzyme, and subsequently acts as the spacer RNA to reconstitute a functional Cas12a/crRNA complex. This two-step, sequence-specific verification substantially enhances detection fidelity by minimizing off-target binding. Through multistage amplification combining CHA, DNAzyme catalysis, transcriptional amplification, and Cas12a-mediated *trans*-cleavage, the assay achieves exceptional sensitivity, with a detection limit as low as 0.52 fM for miRNA-193 and a wide linear range from 1 fM to 100 pM. It demonstrates high specificity by effectively discriminating single-base mismatches, and performs robustly in spiked human serum, yielding recovery rates of 97.3−107.2%. Moreover, results correlate closely with RT-qPCR, confirming reliability in complex matrices. This work presents a versatile and robust biosensing platform that not only offers a promising tool for POD-related miRNA analysis, but also establishes a modular framework adaptable for detecting diverse nucleic acid targets in point-of-care diagnostics.



Downloaded via 223.104.5.81 on May 5, 2026 at 13:45:40 (UTC).
See https://pubs.acs.org/sharingguidelines for options on how to legitimately share published articles.

1. INTRODUCTION

Postoperative delirium (POD) is a neurocognitive disorder characterized by rapid fluctuations in attention, awareness, and cognition following anesthesia and surgery.[1−3] It occurs frequently in elderly patients, with incidence rates ranging from 8% to 70%, depending on factors such as the type of surgical procedure. POD prolongs hospital stays and is associated with increased healthcare costs. Reported 30 day mortality rates reach 7−10% in patients with POD, compared to only 1% in those without delirium.[4] These outcomes underscore the clinical and societal importance of elucidating the mechanisms of POD, identifying specific biomarkers, and developing targeted therapeutics. MicroRNAs (miRNAs) are small noncoding RNA molecules, approximately 22 nucleotides in length, that regulate gene expression post-transcriptionally through sequence-specific interactions.[5−7] By binding to mRNAs, miRNAs modulate their stability and translation, playing pivotal roles in diverse biological processes. Emerging evidence suggests that peripheral surgical trauma and anesthesia contribute to POD onset, implicating circulating molecules such as small RNAs in distal regulatory functions.[8,9] Consequently, blood-based miRNAs represent promising, minimally invasive biomarkers for patients undergoing major surgery. Hence, there is an urgent need to develop accurate and efficient analytical methods for miRNA detection.

The small size, low abundance, and high sequence homology among miRNAs demand detection techniques with exceptional sensitivity and specificity. Currently, quantitative reverse transcription-polymerase chain reaction (RT-qPCR) is the gold standard due to its high sensitivity and specificity; however, its reliance on expensive instrumentation and skilled personnel limits widespread adoption.[10−12] Therefore, developing innovative alternative detection technologies is imperative to address the need for rapid, cost-effective, and user-friendly assays. Isothermal amplification methods, such as loop-mediated isothermal amplification (LAMP),[13] catalytic hairpin assembly (CHA),[14−16] and recombinase polymerase amplification (RPA),[17,18] have attracted considerable interest. Among these, CHA is an enzyme-free, isothermal signal-

Received: February 1, 2026
Revised: March 19, 2026
Accepted: April 9, 2026
Published: April 13, 2026



© 2026 The Authors. Published by American Chemical Society

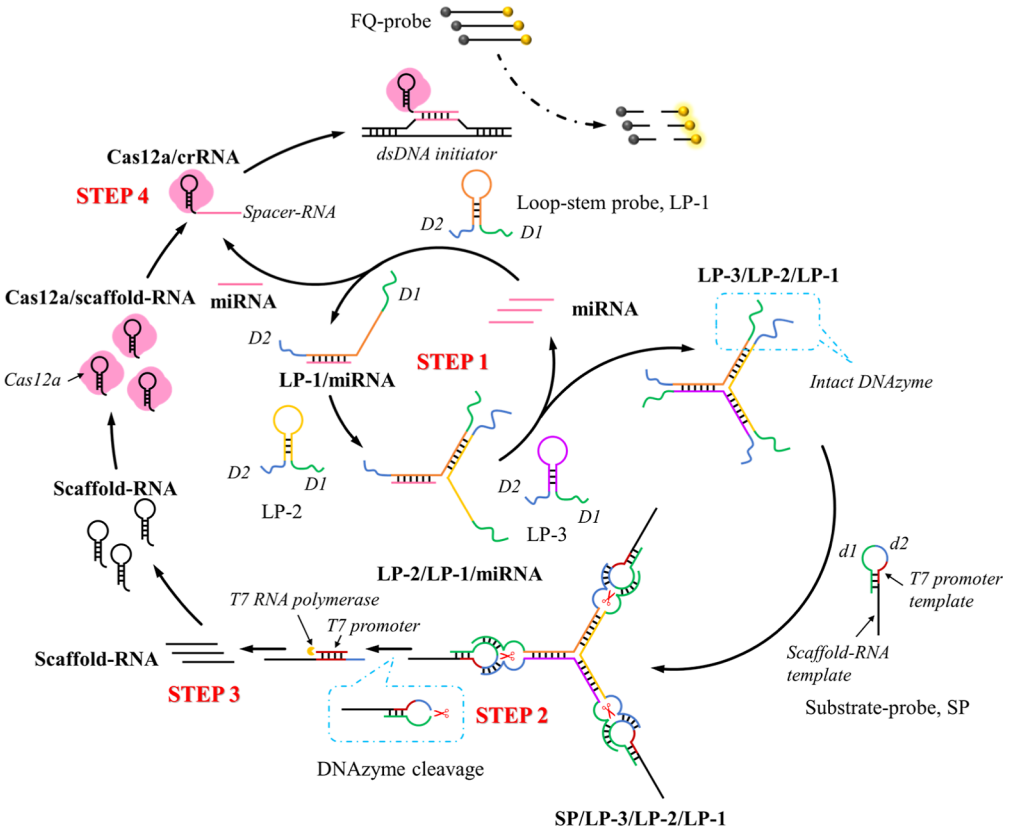


Figure 1. Working mechanism of the proposed method for accurate and sensitive miRNA analysis.

amplification strategy that enables programmable molecular recognition and cascade hybridization reactions with rapid kinetics.[19] Nevertheless, CHA-based methods are often limited by relatively low specificity.

To enhance accuracy, sensitivity, and selectivity, isothermal amplification is frequently combined with other molecular tools.[20,21] The CRISPR/Cas system, originally evolved as a bacterial immune system, has emerged as a powerful platform for nucleic acid detection.[22,23] Integrating CRISPR/Cas with isothermal amplification has led to several highly sensitive diagnostic assays, such as the Cas13-based SHERLOCK (Specific High-sensitivity Enzymatic Reporter Unlocking)[24] and the Cas12a-based DETECTR (DNA Endonuclease-Targeted CRISPR Trans Reporter).[25] Cas12a, a class 2 type V RNA-guided DNA endonuclease, recognizes double-stranded DNA containing a protospacer-adjacent motif ("TTTN") via a single CRISPR RNA (crRNA), inducing PAM-distal cleavage (*cis*-cleavage).[26,27] Moreover, upon target recognition, Cas12a exhibits collateral *trans*-cleavage activity, nonspecifically degrading single-stranded DNA reporters. This property has been widely exploited in molecular diagnostics. Recently, split-crRNA designs have further advanced CRISPR-Cas12a detection capabilities.[28,29] In this approach, the crRNA is divided into two components: a constant scaffold-RNA and a variable spacer-RNA. Studies demonstrate that these fragments can reassemble with Cas12a to form an active complex with *trans*-cleavage efficiency comparable to that of canonical Cas12a system.

To address the aforementioned challenges in miRNA detection, particularly the trade-off between sensitivity and specificity in existing isothermal amplification platforms, we herein propose a novel integrated sensing strategy that leverages the programmable specificity of split crRNA. By coupling catalytic hairpin assembly (CHA)-mediated reassembly of split DNAzyme with T7 RNA polymerase-driven transcription of scaffold RNA and Cas12a/crRNA reconstitution, we constructed a highly sensitive and specific fluorescent assay for miRNA. In this design, the target miRNA initiates CHA, leading to the assembly of an intact DNAzyme that cleaves a substrate to expose a T7 promoter. The exposed promoter then triggers transcription of scaffold RNA, which combines with the same miRNA (acting as spacer RNA) and Cas12a to form a functional split-crRNA/Cas12a complex. Upon activation by a dsDNA initiator, the reconstituted Cas12a exhibits robust *trans*-cleavage activity, repeatedly cleaving fluorescence-quencher (FQ) reporters to generate an amplified fluorescent signal. This cascade architecture confers two key advantages: first, the dual recognition of the same miRNA molecule, both as CHA initiator and as spacer RNA for Cas12a/crRNA assembly, significantly enhances detection specificity; second, the integration of CHA, T7 transcription, and Cas12a *trans*-cleavage enables multistage signal amplification, yielding exceptional sensitivity. Collectively, this method not only offers a promising tool for accurate quantification of POD-related miRNAs, but also establishes a modular framework that can be adapted for the detection of various nucleic acid targets in point-of-care and resource-limited settings, thereby advancing the development of next-generation molecular diagnostics.

2. MATERIALS AND METHODS

2.1. Reagents and Materials

All DNA oligonucleotides were synthesized and purified by Tsingke Biotech Co., Ltd. (Beijing, China). RNA sequences were prepared

https://doi.org/10.1021/acsomega.6c01211
ACS Omega 2026, 11, 24705−24713

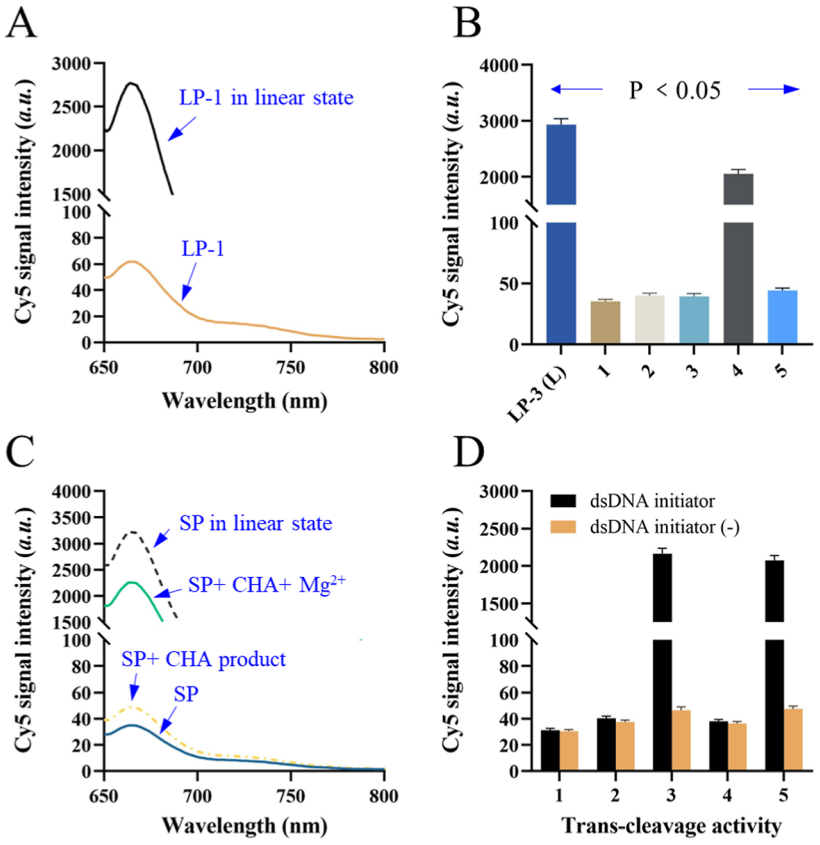


Figure 2. Construction of the sensing platform and feasibility analysis. (A) Cy5 fluorescence spectrum of the LP-1 before and after being assembled to stem-loop structure. (B) Cy5 signal intensity of the LP-3 during the CHA process. LP-3 (L), linear LP-3 (as control); Column 1, LP-3 (stem-loop structure); column 2, LP-3+ LP-1; column 3, LP-3+ LP-2; column 4, LP-3+ LP-2+ LP-1+ miRNA; column 5, LP-3+ miRNA. (C) Cy5 fluorescence spectrum of the SP during the CHA product based cleavage process. DEPC water was used in the Mg^{2+}-free condition to eliminate any potential interference from buffer-derived ions. (D) Cy5 signal intensity of the FQ-probe when Cas12a/split-crRNA or Cas12a/intact-crRNA were used. Column 1, FQ-probe; column 2, FQ-probe + Cas12a; column 3, FQ-probe + Cas12a + intact crRNA; column 4, FQ-probe + Cas12a + scaffold-RNA; column 5, FQ-probe + Cas12a + scaffold-RNA + spacer-RNA (miRNA). All bar graph data are presented as mean ± SD from three independent experiments (n = 3).

and purified by Sangon Biotech Co., Ltd., Shanghai, China (Shanghai, China); detailed sequences are listed in Table S1. The DNAzyme was designed according to former researches.[30,31] EnGen Lba Cas12a (Cpf1) was purchased from New England Biolabs (Ipswich, MA, USA). T7 RNA polymerase and NTPs were sourced from Beyotime Biotechnology (Shanghai, China), and the RNase inhibitor was obtained from Takara Bio (Dalian, China).

2.2. Preparation of Loop Probes and Stem Probes

Stem-loop probes (LP and SP probes) were prepared by thermal annealing. As an example, LP-1 (1 μM, 10 μL) was first heated at 95 °C for 5 min and then slowly cooled to room temperature at a rate of 0.1 °C/s to facilitate proper folding.

2.3. Detection Procedure

The assay was performed in a 50 μL reaction mixture. First, 5 μL each of LP-1, LP-2, LP-3, and SP probes (all at 500 nM) were mixed with 5 μL of target miRNA, and the volume was adjusted to 25 μL with nuclease-free water. The mixture was incubated at room temperature for 30 min to allow catalytic hairpin assembly (CHA). Subsequently, 5 μL of T7 promoter (100 nM), 2 μL of T7 RNA polymerase (1.5 U/μL), 2 μL of NTP mix (10 mM each), and 6 μL of 1× NEBuffer (containing 50 mM NaCl, 10 mM Tris−HCl, 10 mM $MgCl_2$, 100 μg/mL BSA, pH 7.9) were added, and the total volume was brought to 40 μL with nuclease-free water. The reaction was incubated at 37 °C for another 30 min to enable T7 RNA polymerase-driven transcription of scaffold-RNA. Finally, 2 μL of Cas12a protein (20 nM), 2 μL of FQ-labeled reporter (1 μM), and 2 μL of dsDNA initiator (100 nM) were introduced, and the volume was adjusted to 50 μL with nuclease-free water. The mixture was incubated at 37 °C for 60 min, after which the fluorescence intensity was measured at 670 nm (excitation at 635 nm). All experiments were performed in triplicate, and the data are presented as the mean ± standard deviation (SD).

3. RESULTS AND DISCUSSION

3.1. Principle of the Proposed miRNA Detection Assay

The working principle of the established miRNA-sensing platform is schematically depicted in Figure 1. The assay integrates four sequential molecular events: (1) miRNA-triggered catalytic hairpin assembly leading to reassembly of split DNAzyme; (2) DNAzyme-mediated cleavage of a substrate probe (SP); (3) T7 RNA polymerase-driven transcription of scaffold-RNA; and (4) *trans*-cleavage activity of reconstituted Cas12a/crRNA, resulting in fluorescent signal amplification. Specifically, in the CHA module, three stem-loop-structured probes (LP-1, LP-2, and LP-3) were designed, each functionalized at their 3′ and 5′ ends with a fragment of split DNAzyme: D1 (split DNAzyme-1) and D2 (split DNAzyme-2). The target miRNA hybridizes to the toehold region of LP-1, initiating strand displacement and unfolding of the stem. This event triggers a cascade of CHA-mediated hybridization among LP-1, LP-2, and LP-3, ultimately bringing D1 and D2 into close proximity to reconstitute an intact DNAzyme. Subsequently, the assembled DNAzyme hybridizes

https://doi.org/10.1021/acsomega.6c01211
ACS Omega 2026, 11, 24705−24713

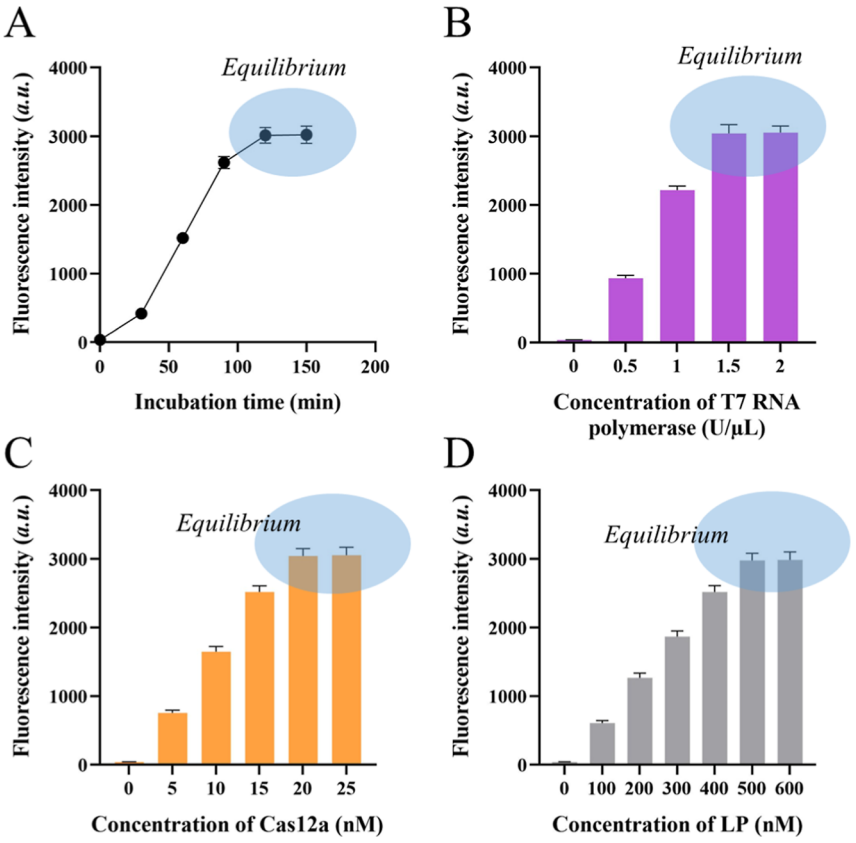


Figure 3. Optimization of experimental parameters. Cy5 fluorescence intensity of the method when detecting target miRNA with different incubation time (A), T7 RNA polymerase concentration (B), Cas12a concentration (C), and LP concentration (D). All bar graph data are presented as mean ± SD from three independent experiments (n = 3).

to the substrate probe (SP) via complementary regions "d1" and "d2" on SP, forming a stable DNAzyme−substrate complex. In the presence of Mg^{2+}, the DNAzyme cleaves the loop region of SP at a specific ribonucleotide site, generating a nick that exposes a previously concealed T7 promoter template sequence. The T7 promoter sequence hybridizes with the T7 promoter template which then serves as a template for T7 RNA polymerase to transcribe multiple copies of scaffold-RNA. The transcribed scaffold-RNA associates with Cas12a protein to form a Cas12a/scaffold-RNA intermediate complex. Notably, the same target miRNA molecule, already involved in the initial CHA step, acts as the spacer-RNA to reconstitute a fully functional Cas12a/crRNA. Upon recognition of a dsDNA initiator, the Cas12a/crRNA is activated and exhibits robust *trans*-cleavage activity, nonspecifically cleaving fluorescence-quencher (FQ)-labeled ssDNA reporters. This repetitive cleavage releases fluorescent reporters from their quenched state, resulting in a cumulative increase in fluorescence intensity that can be quantitatively measured, thereby providing a sensitive readout correlated with the initial miRNA concentration.

3.2. Feasibility Analysis of the Catalytic Hairpin Assembly of Split DNAzyme Cleavage Induced Transcription of Split crRNA Based Fluorescent Assay

To validate the operational viability of the proposed cascade reaction, we systematically interrogated the functionality of each key module. The accurate assembly of linear LPs into stem-loop structure is essential for specific miRNA recognition and subsequent initiation of CHA. We therefore first examined the conformational assembly of the designed LPs using fluorescence spectroscopy. Taking LP-1 as an example, it was dual-labeled with a Cy5 fluorophore at one terminus and a complementary Black Hole Quencher (BHQ) at the other. As shown in Figures 2A and S1, folding into its predesigned stem−loop conformation led to a pronounced decrease in Cy5 fluorescence intensity, indicative of efficient intramolecular quenching due to spatial proximity between the fluorophore and quencher. Similar fluorescence quenching profiles were obtained for LP-2 and LP-3 (Figures S2 and S3, Supporting Information), confirming their successful formation of stable hairpin structures.

We next investigated the feasibility of the miRNA-initiated CHA cascade using a BHQ-quenched Cy5-labeled LP-3. As presented in Figure 2B, the folded LP-3 alone exhibited low background fluorescence. The addition of target miRNA alone, or miRNA together with only LP-1 or LP-2, did not induce a notable fluorescence increase. In contrast, a significant fluorescence enhancement was observed only when all three LPs (LP-1, LP-2, and LP-3) were present together with the target miRNA. This result clearly demonstrates that the complete CHA cascade is specifically triggered by the target miRNA, leading to progressive unfolding of LP-3 and consequent displacement of the quencher, thereby restoring the Cy5 fluorescence signal.

Subsequently, the catalytic cleavage activity of the reassembled DNAzyme on the substrate probe (SP) was verified. The SP was similarly dual-labeled with Cy5 and BHQ. In its folded state, SP displayed low fluorescence due to efficient quenching (Figures 2C and S4). Incubation of SP with

https://doi.org/10.1021/acsomega.6c01211
ACS Omega 2026, 11, 24705−24713

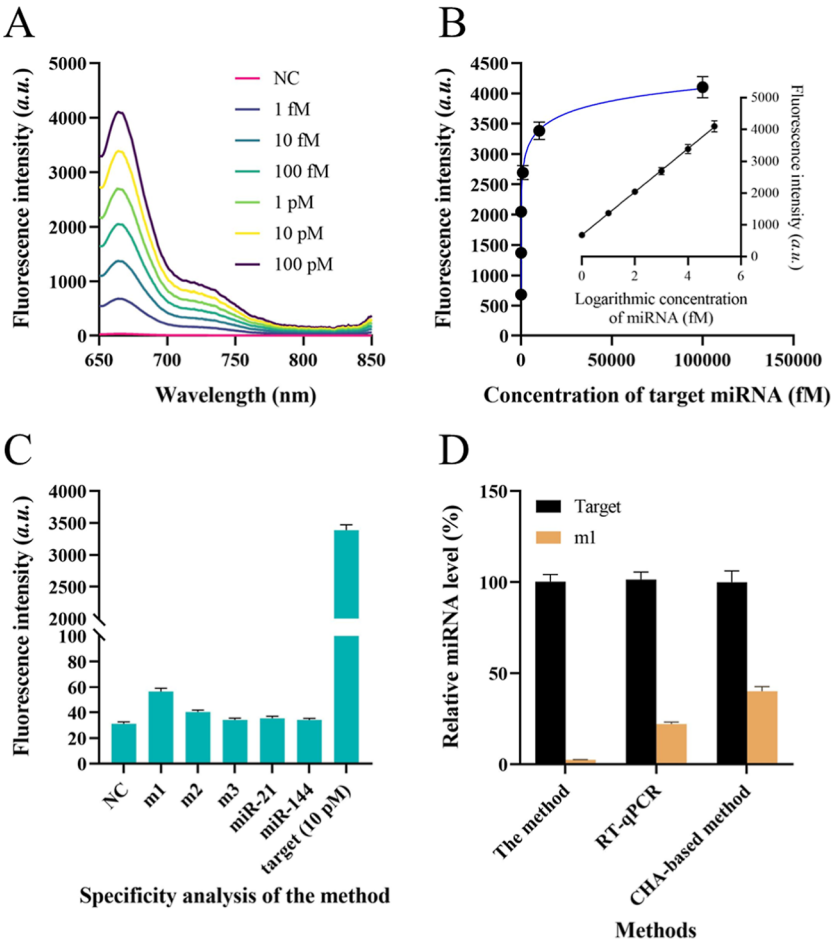


Figure 4. Detection performance of the method. (A) Fluorescent spectrum of the method when detecting different concentrations of miRNA-193. (B) Relation between the peak Cy5 signal intensity and the concentration of target miRNA. (C) Cy5 fluorescence responses of the method upon detection of mismatched sequences (m1, m2, and m3, representing single-base, double-base, and three-base mismatch variants, respectively) and interfering miRNA. (D) Recovered m1 level by the method, RT-qPCR, and former method. All bar graph data are presented as mean ± SD from three independent experiments (n = 3).

the CHA product (containing the reassembled DNAzyme) in the absence of Mg^{2+} yielded no significant fluorescence increase, which can be attributed to the Mg^{2+}-dependent nature of DNAzyme catalysis, the absence of this essential cofactor leaves the DNAzyme inactive and prevents SP cleavage. Upon addition of Mg^{2+}, however, a pronounced fluorescence recovery was observed. This confirms that the CHA-assembled DNAzyme retains its designed enzymatic function: it specifically binds to the complementary "d1" and "d2" regions on SP and, in the presence of Mg^{2+}, cleaves the ribonucleotide site within the loop. This cleavage event permanently separates the fluorophore from the quencher, generating a stable and amplified fluorescent signal. Collectively, these fluorescence-based experiments substantiate the stepwise feasibility of our design: (i) correct folding of all nucleic acid components, (ii) target-specific initiation of the CHA cascade, and (iii) Mg^{2+}-dependent catalytic activity of the reassembled DNAzyme for substrate cleavage. These foundational results confirm the core operational mechanism of the assay and provide a solid basis for further evaluation of analytical performance, including sensitivity, specificity, and applicability in complex biological matrices.

We then assessed the *trans*-cleavage activity of Cas12a/split-crRNA versus that of Cas12a/crRNA by monitoring fluorescence from an FQ-probe. The Cas12a/split-crRNA complex contained Cas12a protein, in vitro-transcribed scaffold-RNA, and target miRNA serving as spacer-RNA, whereas the Cas12a/crRNA complex consisted of Cas12a protein and intact crRNA. As illustrated in Figure 2D, the fluorescence signal increased sharply with Cas12a/split-crRNA, reaching a level comparable to that observed with Cas12a/crRNA, indicating similar *trans*-cleavage efficiencies between the two complexes. In contrast, negligible signal was detected with Cas12a/scaffold-RNA or Cas12a/miRNA alone, confirming that both scaffold-RNA and spacer-RNA are required for efficient Cas12a-mediated *trans*-cleavage.

3.3. Optimization of Experimental Parameters

To achieve optimal analytical performance, key experimental parameters influencing the cascade reaction efficiency were systematically optimized. Four critical variables were examined: total reaction duration, concentrations of T7 RNA polymerase and Cas12a protein, and the concentration of linear probes (LPs). Total reaction time was first varied from 0 to 150 min. As depicted in Figure 3A, fluorescence intensity increased progressively up to 120 min, after which it plateaued without further significant enhancement. This kinetic behavior suggests that the multistep cascade, comprising CHA, DNAzyme cleavage, transcription, and Cas12a-mediated *trans*-cleavage, approaches completion within this period.

https://doi.org/10.1021/acsomega.6c01211
ACS Omega 2026, 11, 24705−24713

Accordingly, a total reaction time of 120 min was selected for all subsequent assays to maximize signal output while maintaining a practical assay duration.

Next, the concentration of T7 RNA polymerase, responsible for transcribing scaffold-RNA from the liberated promoter, was optimized. Figure 3B presents the relationship between fluorescence intensity and polymerase concentration. Signal strength increased with enzyme concentration up to 1.5 U/μL, beyond which a gradual decline was observed. The initial rise likely reflects enhanced transcription efficiency and elevated scaffold-RNA production, whereas the subsequent decrease at higher concentrations may result from nonspecific interactions or steric interference that could impede downstream complex assembly. Hence, 1.5 U/μL was identified as the optimal T7 RNA polymerase concentration.

The concentration of Cas12a protein, which executes the final *trans*-cleavage signal amplification step, was also evaluated. As shown in Figure 3C, fluorescence intensity rose with Cas12a concentration and saturated near 20 nM. Further increases did not yield additional signal gain, indicating that either the reconstituted Cas12a/crRNA complexes or the FQ reporter substrate became limiting under the tested conditions. Therefore, 20 nM Cas12a was chosen as the optimal concentration to ensure efficient cleavage activity while conserving reagents.

Finally, the concentration of the LP probes, which form the basis of the CHA cascade, was refined. Figure 3D demonstrates that fluorescence intensity increased with LP concentration, peaking at 500 nM, consistent with more efficient CHA initiation and DNAzyme reassembly. Above this concentration, the signal stabilized, suggesting that the target miRNA or subsequent reaction components became rate-limiting. Excessively high probe concentrations may also elevate background signal due to probe instability or nonspecific binding. Consequently, a concentration of 500 nM for each LP was adopted for further experiments.

3.4. Detection Performance of the Method

Under optimized conditions, the analytical sensitivity of the assay was evaluated by measuring the fluorescence response to varying concentrations of the target miRNA-193. As shown in Figure 4A, fluorescence intensity increased in a clear concentration-dependent manner, with higher miRNA levels yielding stronger signals. A linear relationship was observed between the fluorescence intensity (F) at 670 nm and the logarithm of miRNA-193 concentration (C) across a broad dynamic range of 1 fM to 100 pM (Figure 4B). The corresponding linear regression equation was F = 679.9 × lgC +680.5 (C in fM), with a correlation coefficient (R^2) of 0.9928. The limit of detection (LOD), calculated using the 3 δ/slope criterion (where δ represents the standard deviation of the blank signal), was determined to be 0.52 fM. This result underscores the exceptional sensitivity achieved through the multistage amplification cascade.

To evaluate specificity, the fluorescence signal generated by the fully matched target (miRNA-193) was compared with signals from several control sequences (Figure 4C). These included four mismatch variants (m1 to m3, containing one to three base substitutions within the miRNA-193 sequence, respectively) and two unrelated miRNAs (miRNA-21 and miRNA-144). A pronounced fluorescence increase was observed only in the presence of perfectly complementary miRNA-193. Notably, even a single-base mismatch (m1) caused a drastic reduction in signal, highlighting the assay's high sequence-discrimination capability. This stringent specificity originates from the dual-recognition design: the target miRNA must hybridize correctly twice—first to initiate the CHA cascade, and subsequently to act as the spacer-RNA for Cas12a/crRNA reconstitution. This built-in verification step substantially enhances detection fidelity.

To further benchmark the gain in specificity afforded by this design, a comparative analysis was performed. The discrimination factor between miRNA-193 and its single-base mismatch variant (m1) was quantified using the proposed method, conventional RT-qPCR, and a previously reported CHA-based assay. As illustrated in Figure 4D, the signal recovery for mis-RNA-1 relative to miRNA-193 was only about 3.21% with our method. This value is markedly lower than those obtained by RT-qPCR (~21.2%) or the earlier CHA method (~41.5%), confirming a superior ability to differentiate single-nucleotide variations. Collectively, these results demonstrate that the integrated dual-recognition strategy effectively suppresses false-positive signals from closely related sequences, thereby significantly improving specificity over conventional single-step recognition or amplification approaches.

3.5. Clinical Application Potential of the Method

The inherent complexity of clinical sample matrices presents a significant challenge to the practical application of biosensing technologies. To evaluate the clinical applicability of the proposed method, miRNA-193 was spiked into normal human serum at four different concentrations to mimic real clinical conditions. The detected miRNA-193 levels closely matched the known spiked amounts, with recovery rates ranging from 97.3% to 107.2% and relative standard deviations (RSDs) between 1.2% and 4.3%. These results demonstrate that the split crRNA-based Cas12a fluorescence assay is robust against matrix interference, offering a reliable platform for highly sensitive detection of miRNA-193 in clinical environments.

Subsequently, miRNA concentrations in the prepared samples were quantified using both the developed assay and RT-qPCR. Figure 5 shows strong agreement between the results obtained with the two methods, particularly in determining the relative expression levels of miRNA-193. The high consistency (R^2 = 0.9933) indicates that the present assay effectively minimizes interference from serum components and is suitable for real-sample analysis.

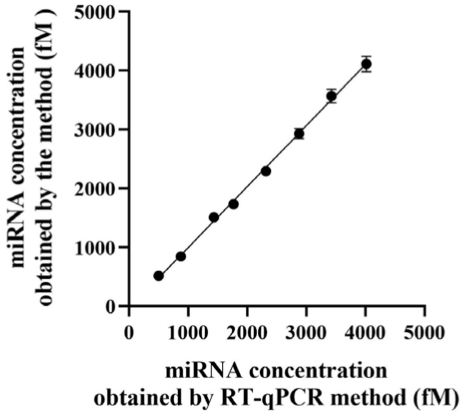


Figure 5. Correlation between the miRNA concentration obtained by the method and the RT-qPCR method. All bar graph data are presented as mean ± SD from three independent experiments (n = 3).

https://doi.org/10.1021/acsomega.6c01211
ACS Omega 2026, 11, 24705−24713

4. CONCLUSION

In summary, we have successfully developed a novel and integrated fluorescent biosensor for the sensitive and specific detection of miRNA, utilizing a cascade signal amplification strategy that combines catalytic hairpin assembly, split DNAzyme cleavage, T7 RNA polymerase-mediated transcription, and CRISPR-Cas12a *trans*-cleavage. This work directly addresses the critical challenge of achieving both high sensitivity and stringent specificity in miRNA diagnostics, a trade-off often encountered in existing isothermal amplification platforms.

The core innovation of this method lies in its dual-recognition mechanism for the same target miRNA molecule. The target miRNA first acts as the initiator to trigger the CHA cascade, leading to the reassembly of an active split DNAzyme. Subsequently, the same miRNA molecule serves as the spacer-RNA, combining with the Cas12a/scaffold-RNA complex to reconstitute a fully functional Cas12a/crRNA effector. This two-step, sequence-specific verification process introduces an inherent fidelity check, substantially reducing off-target binding and false-positive signals caused by single-nucleotide polymorphisms or homologous miRNA family members. This design effectively overcomes the common limitation of low specificity associated with traditional CHA-based methods. Complementing this enhanced specificity, the assay achieves remarkable sensitivity through multistage signal amplification. The initial CHA provides the first level of amplification, which is followed by the catalytic activity of the DNAzyme, the transcriptional amplification by T7 RNA polymerase, and finally the potent, nonspecific *trans*-cleavage activity of Cas12a. Under optimized conditions, this synergistic cascade enabled the detection of miRNA-193 with a limit of detection as low as 0.52 fM and a wide linear dynamic range spanning 5 orders of magnitude. The method demonstrated superior specificity in discriminating target miRNAs from single-base mismatch variants, outperforming conventional RT-qPCR and other reported CHA-based assays. Furthermore, the practical utility of the biosensor was validated through spike-and-recovery experiments in human serum, yielding satisfactory recoveries and low variability. The results showed excellent correlation with the gold-standard RT-qPCR, confirming its robustness against complex matrix interference and its potential for reliable analysis in clinical settings. Notably, by simply reprogramming the recognition sequences in the hairpin probes, the proposed strategy can be readily extended to detect other POD-related miRNAs or any miRNA of interest, further demonstrating its adaptability and broad utility in biomarker analysis.

Despite its high sensitivity and specificity, the proposed method has certain limitations. The current design is optimized for single-target detection and does not support multiplexed miRNA analysis, which may restrict its application in scenarios requiring simultaneous profiling of multiple biomarkers. Additionally, although the assay involves only two operational steps, the overall reaction time of 120 min and the requirement for multiple reagent additions may pose challenges for point-of-care implementation. Future efforts will focus on addressing these limitations by integrating microfluidic chip technology to accelerate reaction kinetics and reduce overall assay time. Furthermore, adopting multichannel or array-based designs will enable high-throughput, multiplexed detection of multiple miRNA targets, thereby enhancing the clinical utility and translational potential of this platform for point-of-care diagnostics.

In conclusion, this work presents a powerful and versatile molecular tool that not only provides a promising solution for the accurate quantification of POD-related miRNAs but also establishes a generalizable modular framework. The design principle of integrating a dual-recognition step with multienzyme amplification can be readily adapted for the detection of various nucleic acid targets, paving the way for the development of next-generation point-of-care diagnostics with enhanced reliability for clinical and research applications.

■ ASSOCIATED CONTENT

Supporting Information

The Supporting Information is available free of charge at https://pubs.acs.org/doi/10.1021/acsomega.6c01211.

Sequences of the oligonucleotides (Table S1); Supplemented details; Cy5 signal intensity of the LP-1 before and after being assembled to stem-loop structure (Figure S1); Cy5 signal intensity of the LP-2 before and after being assembled to stem-loop structure (Figure S2); Cy5 signal intensity of the LP-3 before and after being assembled to stem-loop structure (Figure S3); Cy5 fluorescence spectrum of the SP during the CHA product based cleavage process (Figure S4) (PDF)

■ AUTHOR INFORMATION

Corresponding Author

Baojun Zhang − *Department of Anesthesiology and Perioperative Medicine, Xinxiang Central Hospital (The Fourth Clinical College of Henan Medical University), Xinxiang City 453000, China;* orcid.org/0009-0005-5582-6779; Phone: +8618637310589; Email: 466542552@qq.com

Authors

Lihua Wang − *Department of Anesthesiology and Perioperative Medicine, Xinxiang Central Hospital (The Fourth Clinical College of Henan Medical University), Xinxiang City 453000, China*

Huihui Li − *Department of Anesthesiology and Perioperative Medicine, Xinxiang Central Hospital (The Fourth Clinical College of Henan Medical University), Xinxiang City 453000, China*

Kai Wang − *Department of Anesthesiology and Perioperative Medicine, Xinxiang Central Hospital (The Fourth Clinical College of Henan Medical University), Xinxiang City 453000, China*

Jinge Ma − *Department of Anesthesiology and Perioperative Medicine, Xinxiang Central Hospital (The Fourth Clinical College of Henan Medical University), Xinxiang City 453000, China*

Guosheng Liu − *Department of Anesthesiology and Perioperative Medicine, Xinxiang Central Hospital (The Fourth Clinical College of Henan Medical University), Xinxiang City 453000, China*

Ning Li − *Department of Anesthesiology and Perioperative Medicine, Xinxiang Central Hospital (The Fourth Clinical College of Henan Medical University), Xinxiang City 453000, China*

Complete contact information is available at:

https://doi.org/10.1021/acsomega.6c01211
ACS Omega 2026, 11, 24705−24713

https://pubs.acs.org/10.1021/acsomega.6c01211

Author Contributions

B.Z.: Supervision, Data curation, Funding acquisition, Conceptualization, Methodology, Reviewing original draft. L.W.: Software, Investigation, Methodology, Writing original manuscript. H.L., K.W., J.M., G.L., and N.L.: Methodology, Formal analysis.

Notes

The authors declare no competing financial interest.

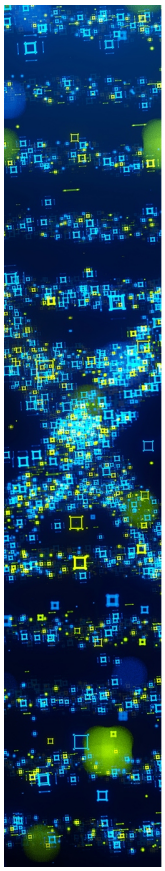
■ ACKNOWLEDGMENTS

This work was supported by Supported by the Henan Provincial Joint Construction Project (Number: LHGJ20240840).

■ REFERENCES

(1) Swarbrick, C. J.; Partridge, J. S. L. Evidence-based strategies to reduce the incidence of postoperative delirium: a narrative review. *Anaesthesia* **2022**, *77* (S1), 92−101.
(2) Thedim, M.; Vacas, S. Postoperative Delirium and the Older Adult: Untangling the Confusion. *J. Neurosurg. Anesthesiol* **2024**, *36* (3), 184−189.
(3) Urbanek, L.; Urbankova, P.; Satinsky, I.; Travnicek, T.; Penka, I.; Hruda, J. Postoperative delirium. *Rozhl. Chir.* **2023**, *102* (10), 381−386.
(4) Xiao, M. Z.; Liu, C. X.; Zhou, L. G.; Yang, Y.; Wang, Y. Postoperative delirium, neuroinflammation, and influencing factors of postoperative delirium: A review. *Medicine (Baltimore)* **2023**, *102* (8), No. e32991.
(5) Ma, X.; Zhou, F.; Yang, D.; Chen, Y.; Li, M.; Wang, P. miRNA Detection for Prostate Cancer Diagnosis by miRoll-Cas: miRNA Rolling Circle Transcription for CRISPR-Cas Assay. *Anal. Chem.* **2023**, *95* (35), 13220−13226.
(6) Xiong, Y.; Xu, J.; Zhang, D.; Wu, S.; Li, Z.; Zhang, J.; Xia, Z.; Xia, P.; Xia, C.; Tang, X.; Liu, X.; Liu, J.; Yu, P. MicroRNAs in Kawasaki disease: An update on diagnosis, therapy and monitoring. *Front. Immunol.* **2022**, *13*, 1016575.
(7) Wu, Y.; Li, Q.; Zhang, R.; Dai, X.; Chen, W.; Xing, D. Circulating microRNAs: Biomarkers of disease. *Clin. Chim. Acta* **2021**, *516*, 46−54.
(8) Xu, M.; Chen, Y.; Lin, Y.; Wang, D.; Zheng, X. Serum-derived exosomal microRNAs as biomarkers for postoperative delirium. *Front. Neurosci.* **2025**, *19*, 1525230.
(9) Gao, R.; Chen, C.; Zhao, Q.; Li, M.; Wang, Q.; Zhou, L.; Chen, E.; Chen, H.; Zhang, Y.; Cai, X.; Liu, C.; Cheng, X.; Zhang, S.; Mao, X.; Qiu, Y.; Gan, L.; Yu, H.; Liu, J.; Zhu, T. Identification of the Potential Key Circular RNAs in Elderly Patients With Postoperative Cognitive Dysfunction. *Front. Aging Neurosci.* **2020**, *12*, 165.
(10) Buglyo, G.; Magyar, Z.; Romicsne Gorbe, E.; Banusz, R.; Csoka, M.; Micsik, T.; Berki, Z.; Varga, P.; Sapi, Z.; Nagy, B. Quantitative RT-PCR-based miRNA profiling of blastemal Wilms' tumors from formalin-fixed paraffin-embedded samples. *J. Biotechnol.* **2019**, *298*, 11−15.
(11) Kramer, M. F. Stem-loop RT-qPCR for miRNAs. *Curr. Protoc. Mol. Biol.* **2011**, *95*, 1934−3647.
(12) Xue, Y.; Wang, K.; Jiang, Y.; Dai, Y.; Liu, X.; Pei, B.; Li, H.; Xu, H.; Zhao, G. An ultrasensitive and multiplexed miRNA one-step real time RT-qPCR detection system and its application in esophageal cancer serum. *Biosens. Bioelectron.* **2024**, *247*, 115927.
(13) Liu, X.; Peng, H.; Ye, X.; Zhang, X.; Xu, G.; Zhao, X. A Versatile Colorimetric Diagnostic Platform Based on Primer Exchange Reaction Cascades Driven Loop-Mediated Isothermal Amplification. *Anal. Chem.* **2025**, *97* (16), 9000−9007.
(14) Luo, X.; Tan, R.; Xia, Z.; Yue, W.; Peng, J.; Yuan, X.; Wang, M.; Li, P.; He, Y. Catalytic hairpin assembly-mediated SERS biosensor for double detection of MiRNAs using gold nanoclusters-doped COF substrate. *Sensors Actuators B: Chem.* **2024**, *401*, 134953.
(15) Ma, F.; Zhang, Q.; Zhang, C. Y. Catalytic Self-Assembly of Quantum-Dot-Based MicroRNA Nanosensor Directed by Toehold-Mediated Strand Displacement Cascade. *Nano Lett.* **2019**, *19* (9), 6370−6376.
(16) Wang, W.; Liu, J.; Wu, L. A.; Ko, C. N.; Wang, X.; Lin, C.; Liu, J.; Ling, L.; Wang, J. Nicking enzyme-free strand displacement ampli fi cation-assisted CRISPR-Cas-based colorimetric detection of prostate-specific antigen in serum samples. *Anal. Chim. Acta* **2022**, *1195*, 339479.
(17) Lobato, I. M.; O'Sullivan, C. K. Recombinase polymerase amplification: Basics, applications and recent advances. *Trends Analyt. Chem.* **2018**, *98*, 19−35.
(18) Bai, Y.; Ji, J.; Ji, F.; Wu, S.; Tian, Y.; Jin, B.; Li, Z. Recombinase polymerase amplification integrated with microfluidics for nucleic acid testing at point of care. *Talanta* **2022**, *240*, 123209.
(19) Mo, L.; Liang, D.; Qin, R.; Mo, M.; Yang, C.; Lin, W. Three-Dimensional CHA-HCR System Using DNA Nanospheres for Sensitive and Rapid Imaging of miRNA in Live Cells and Tissues. *Anal. Chem.* **2023**, *95* (31), 11777−11784.
(20) Zhu, J.; Wang, C.; Huang, T.; Zeng, L.; Niu, Q.; Huang, X.; Chen, H.; Jiang, M.; Deng, B.; Yan, Y.; Liu, X.; Chen, J.; Xie, Y.; Shen, J.; Chen, W.; Gao, Y.; Chen, K.; Lin, X.; Zeng, L.; Li, B.; Song, Y.; Zhu, J.; Li, B. Rapid Detection and Purification of Extracellular Vesicles for Hepatocellular Carcinoma Screening Using a Plasmonic Metasurface Integrated with the Kolmogorov-Arnold Network. *ACS Nano* **2025**, *19* (49), 41557−41570.
(21) Zhu, J.; Xiao, Y.; Huang, X.; Niu, Q.; Zeng, L.; Lin, S.; Jiang, M.; Huang, T.; Chen, H.; Xie, Y.; Gao, Y.; Chen, W.; Yan, Y.; Shen, J.; Chen, K.; Dai, Y.; Zhang, Z.; Zeng, L.; Chen, Y.; Li, B.; Zhu, J.; Li, B. Deep Learning-Powered Nanoplasmonic Biosensing Approach Enables Ultrasensitive Extracellular Vesicles Profiling for Cancer Screening. *Adv. Sci. (Weinh)* **2026**, *13* (2), No. e11337.
(22) Wang, R.; Zhao, X.; Chen, X.; Qiu, X.; Qing, G.; Zhang, H.; Zhang, L.; Hu, X.; He, Z.; Zhong, D.; Wang, Y.; Luo, Y. Rolling Circular Amplification (RCA)-Assisted CRISPR/Cas9 Cleavage (RACE) for Highly Specific Detection of Multiple Extracellular Vesicle MicroRNAs. *Anal. Chem.* **2020**, *92* (2), 2176−2185.
(23) Zhang, G. Z. L.; Zhang, L.; Tong, J.; Zhao, X.; Ren, J. CRISPR-Cas12a enhanced rolling circle amplification method for ultrasensitive miRNA detection. *Microchem. J.* **2020**, *158* (2020), 105239.
(24) Gootenberg, J. S.; Abudayyeh, O. O.; Lee, J. W.; Essletzbichler, P.; Dy, A. J.; Joung, J.; Verdine, V.; Donghia, N.; Daringer, N. M.; Freije, C. A.; Myhrvold, C.; Bhattacharyya, R. P.; Livny, J.; Regev, A.; Koonin, E. V.; Hung, D. T.; Sabeti, P. C.; Collins, J. J.; Zhang, F. Nucleic acid detection with CRISPR-Cas13a/C2c2. *Science* **2017**, *356* (6336), 438−442.
(25) Chen, J. S.; Ma, E.; Harrington, L. B.; Da Costa, M.; Tian, X.; Palefsky, J. M.; Doudna, J. A. CRISPR-Cas12a target binding unleashes indiscriminate single-stranded DNase activity. *Science* **2018**, *360* (6387), 436−439.
(26) Ding, L.; Cao, S.; Qu, C.; Wu, Y.; Yu, S. Ratiometric CRISPR/Cas12a-Triggered CHA System Coupling with the MSRE to Detect Site-Specific DNA Methylation. *ACS Sens* **2024**, *9* (4), 1877−1885.
(27) Long, X.; Li, J.; Luo, T.; Liu, H.; Deng, Z.; Ding, J.; Gong, Z.; Yang, Y.; Zhong, S. CRISPR-Cas12a coupled with cyclic reverse transcription for amplified detection of miRNA. *Chem. Commun. (Camb.)* **2023**, *59* (50), 7763−7766.
(28) Chen, Y.; Wang, X.; Zhang, J.; Jiang, Q.; Qiao, B.; He, B.; Yin, W.; Qiao, J.; Liu, Y. Split crRNA with CRISPR-Cas12a enabling highly sensitive and multiplexed detection of RNA and DNA. *Nat. Commun.* **2024**, *15* (1), 8342.
(29) Zha, C. J.; Zhang, H. S.; He, S.; Zhao, N.; He, L.; Yang, N.; Ying, Z. M. RT-RPA-assisted scaffold RNA transcription amplification activation Cas12a trans-cleavage strategy for one-pot miRNA detection. *Talanta* **2025**, *293*, 128049.
(30) Huang, X.; Li, Z.; Tong, Y.; Zhang, Y.; Shen, T.; Chen, M.; Huang, Z.; Shi, Y.; Wen, S.; Liu, S. Y.; Guo, J.; Zou, X.; Dai, Z.

DNAzyme-Amplified Cascade Catalytic Hairpin Assembly Nanosystem for Sensitive MicroRNA Imaging in Living Cells. *Anal. Chem.* **2023**, *95* (31), 11793−11799.
(31) Li, D.; Xiang, J.; Wang, Y.; Xiang, Y.; Yuan, R. Target-initiated autocatalytic and concatenated DNAzyme/CHA amplification cascades for highly sensitive fluorescent detection of TET1 dioxygenase. *Talanta* **2025**, *293*, 128114.


CAS BIOFINDER DISCOVERY PLATFORM™
STOP DIGGING THROUGH DATA —START MAKING DISCOVERIES
CAS BioFinder helps you find the right biological insights in seconds
Start your search
CAS
A division of the American Chemical Society

https://doi.org/10.1021/acsomega.6c01211
ACS Omega 2026, 11, 24705−24713